PSFC/JA-05-36

The Scrape-Off-Layer in Alcator C-Mod –Transport, Turbulence, and Flows

J.L. Terry, B. LaBombard, B. Lipschultz,
M.J. Greenwald, J.E. Rice, S. J. Zweben[1]

.

[1]Princeton Plasma Physics Laboratory, Princeton, NJ 08543 USA

December 2005

Plasma Science and Fusion Center
Massachusetts Institute of Technology
Cambridge MA 02139 USA

This work was supported by the U.S. Department of Energy, Grant No. DE-FC02-99ER54512. Reproduction, translation, publication, use and disposal, in whole or in part, by or for the United States government is permitted.

The Scrape-Off-Layer in Alcator C-Mod –Transport, Turbulence, and Flows

J.L. Terry, B. LaBombard, B. Lipschultz, M.J. Greenwald, J.E. Rice

Plasma Science and Fusion Center, Cambridge, MA 02131 USA

S. J. Zweben

Princeton Plasma Physics Laboratory, Princeton, NJ 08543 USA

Abstract

Research on the scrape-off-layer plasma of the Alcator C-Mod Tokamak is reviewed. The research has focused on understanding the transport of energy and particles both parallel and perpendicular to the magnetic field. Large differences between the inboard, high-field side scrape-off-layer and the outboard, low-field side are found. On the outboard side large levels of anomalous cross-field transport of heat and particles exist, with important and far-reaching consequences on recycling, power handling, plasma flows, and possibly core-plasma density limits and rotation. The phenomenon of "main-chamber-recycling" is discussed. Parallel and perpendicular transport, together with the heat and particle sources, determine the plasma profiles in the scrape-off-layer, and these profiles show qualitative differences between near scrape-off-layer and far scrape-off-layer regions. Particle transport in the near scrape-off-layer exhibits a strong scaling with collisionality, while transport in the far scrape-off-layer is clearly convective with little obvious dependence on collisionality. The anomalously large magnitudes of perpendicular transport are the result of turbulence. Turbulent structures, "blobs", are largely responsible, and their characteristics have been examined. The turbulent structures are approximately aligned with the field and have $k_{\|} << k_{perp}$. Their characteristic size perpendicular to the field is ~1cm and their characteristic lifetime is ~1-50 μs. The turbulent structures move both radially outward and poloidally at speeds up to ~1 km/s. Evidence that this turbulent transport may play an important role in the core-plasma density limit is presented. Much lower levels of turbulence and no blobs are observed in the high-field-side scrape-off-layer. For single-null magnetic configurations, plasma in the inboard scrape-off-layer appears to be almost entirely a result of plasma flow along field lines from the low-field side. Strong parallel flows with sensitivity to magnetic topology are found, along with strong evidence for momentum coupling between these scrape-off-layer flows and core toroidal rotation.

I. Introduction and Overview

The scrape-off-layer (SOL) is that region of open field lines, just outside the last closed flux surface (LCFS), where plasma physics, atomic physics, and plasma-surface physics interact. A cross-section of the C-Mod plasma, showing the SOL, the main-chamber, outboard limiter, and divertor is presented in Fig. 1. The properties of the SOL play a crucial role in some of the most

important problems in magnetic fusion research. For example, the "widths" of the power and particle scrape-off zone set crucial boundary conditions for the power- and particle-handling demands on the divertor. Additional examples are the fundamental roles that transport within the SOL plays in "helium ash" removal, plasma fueling, and plasma-wall interactions. Unfortunately, the key properties of the SOL cannot at the present time be accurately *predicted* either for present-day tokamaks or for a reactor like ITER by theory or by simulation codes. Thus understanding the SOL remains a topic of importance and intense interest.

Research on Alcator C-Mod has contributed greatly to the present understanding of the SOL. C-Mod's SOL research has focused on *transport* (including flows) because of its fundamental importance in the fusion research issues mentioned above. Probably the most important contributions made by C-Mod results have been the description of the perpendicular transport in the "near" and "far" SOL and the appreciation of the implications of this description (see e.g. Ref. [1]). In particular, work on C-Mod has focused attention on the difference in transport in the near- and far-SOL (defined more precisely below). In the far-SOL the cross-field transport is large and convective. One important consequence of this physics is that the radial e-folding distance of particle fluxes in the SOL is much larger than the corresponding energy fluxes along magnetic field lines. As a result, divertor target and baffle structures, which may necessarily be shaped in a fusion reactor to spread the heat flux over a large surface area (as they are in Alcator C-Mod), may not readily accommodate the total particle flux efflux from the confined plasma; the resultant 'throat' into the divertor may be too narrow. Indeed, the "gap" between the LCFS and flux surfaces outside of the divertor throat may not be large compared to the characteristic width of the density profile in the *far-SOL,* and a strong interaction between the far-SOL plasma

and main-chamber surfaces may result. These and other consequences and contributions will be reviewed in what follows.

This summary is organized around C-Mod's contributions to the present understanding of SOL transport physics. We do not give a comprehensive review of all work done on C-Mod that relates to the SOL. For example, research on impurities in the SOL is not discussed. Instead, we restrict ourselves mainly to SOL transport, turbulence, and flows. Section II discusses the time-averaged characteristics of C-Mod's outboard SOL and their scalings. Some of the consequences of the observed properties are also presented. In section III the "microscopic", time-dependent observations of outboard SOL turbulence and transport are addressed. This turbulent transport determines the time-averaged, macroscopic profiles. ELMs will not be discussed here since they have not been a prominent feature of C-Mod operation to date; type I ELMs are rarely seen on C-Mod, and, while smaller amplitude, higher frequency ELMs do occur in some discharges, they are not typical. The relationship of the outboard SOL turbulence and transport to the operational density limit (the Greenwald limit), n_{GW}, observed universally in tokamaks [2], is discussed in Section IV. Research on the large differences seen between the inboard and outboard SOLs is detailed in Section V. Finally, we review C-Mod's contributions to the topic of plasma flows in the SOL, as well as their connections to core-plasma rotation.

II. Time-averaged Characteristics of the Outboard SOL

Because C-Mod occupies a unique portion of tokamak operational space (high field, high density, small scale lengths), it is important to document some of the key parameters describing C-Mod's SOL. Indeed, its unique or nearly unique parameter space gives it important "leverage"

in determining crucial empirical scaling relations when multi-tokamak databases are assembled and in testing theories of heat or particle transport. To quote a multi-machine study of heat flux scale lengths: the "extreme nature of Alcator C-Mod SOL, at twice the toroidal field of most other machines and with up to an order of magnitude higher separatrix densities, makes it invaluable for extending the testing of [heat flux scale length] scalings" [3]. Although we will not discuss multi-machine SOL scalings here, C-Mod data have been used in a number of studies (see e.g. [3, 4]) and are present in actively maintained international databases.

Most SOL measurements have been made in the outboard SOL, because of easier diagnostic access. However, more recently, measurements of C-Mod's *inboard* SOL, near the midplane, have been made. The important differences that we measure between properties of the inboard and outboard SOL make it clear that the SOL properties are not poloidally symmetric. In this section, unless noted, the characteristics of the outboard, low-field side SOL are presented.

	C-Mod near-SOL	**C-Mod far-SOL**	ref./ comment
n_e ($x10^{19}$ m^{-3})	2-25	0.1-10	[3,4,5,6]
T_e (eV)	20-80	5-20	[4] for $n/n_{GW}<0.5$
λ_{Te}^{perp} (mm)	2-20	7-40	[4,11]
λ_n^{perp} (mm)	3-9	10-∞	[11]
$q_{//}$ (MW/m^2)	$\leq$500	NA	[7]
ρ_s (mm)	0.11-0.43	0.05-0.22	
$L_{//}$ (m)	55-7	40-4	See caption
Neutral pressure (Pa)	NA	0.001-.15	[8]
$\nu^*=L_{//}/\lambda_{ei}$	~2-190	~5-~1000	[3]
$\lambda_n^{perp}/\lambda_{ni}$	~0.2-4	NA	"Neutral Opacity"
β_{perp}	0.3-13$x10^{-4}$	0.02-1.8$x10^{-4}$	Assuming $T_i=T_e$, $n_i=n_e$
n_{sep}/n_{GW}	0.05-0.2	NA	[5,6]

Table I. Dimensional and non-dimensional parameters of the C-Mod outboard SOL. The ranges are those for plasmas within C-Mod's typical operating space. n_{GW} is the "Greenwald" density limit. $L_{//}$ is evaluated as 1/2 of total field-line length, not including field-lines ending on non-toroidally symmetric limiters. The upper limit of $L_{//}$ in the near-SOL is evaluated at ρ=2 mm, i.e. at the 1/e point for the minimum λ_{Te}^{perp}. The neutral mean-free-path, λ_{ni}, is dominated in the near-SOL by charge exchange. Thus we have evaluated λ_{ni} as $v^{neutral}/[n_i<\sigma v>_{cx}]$, with $v^{neutral}$ roughly estimated assuming 3 eV Franck-Condon neutrals. "NA" means "not applicable".

A tabulation of C-Mod SOL parameters is presented in Table I, where both dimensional and non-dimensional quantities are listed. Because, as noted above, there are distinct and important differences between the near- and far-SOL, we list the range of C-Mod values in each. For the purposes of Table I the near-SOL is defined as that region between the separatrix and ρ=5 mm, where ρ is radial coordinate at the outboard midplane of the flux surface on which the measurement is made. The far-SOL is where ρ>5 mm. Toroidally asymmetric limiter surfaces typically exist at ρ~20 mm; thus the outer gap to these surfaces (at the midplane) is typically ~20 mm, significantly greater than the density scrape-off length of the near-SOL, but roughly equal to or less than the scrape-off length of the far-SOL. The dividing point, ρ=5 mm, is somewhat arbitrary, since this is not always constant nor even precisely defined. Nonetheless, the need for a division is evident in the density profiles (see Fig. 2a for example), where there is typically a break in slope in the profile about one *near-SOL* density scrape-off-length outside the separatrix, beyond which the profile is much flatter, i.e. with a larger scale length. An important implication, developed in more detail below, is that the transport is different between the two regions.

A few of the parameters in Table I are worthy of special note, because they are either ITER-relevant, near an extreme for today's tokamaks, or can be varied over a wide range. Those parameters that are especially ITER-relevant are the parallel heat flux, $q_{\|}$, the collisionality, ν^* (the ratio of the parallel connection length to the electron-ion mean free path), and the opacity to neutral penetration (defined as the density gradient scale length, λ_n^{perp}, normalized by the neutral mean-free-path, λ_{ni}). C-Mod accesses both the largest values (and closest to those expected for ITER) and a large range for all three of these parameters. Because of C-Mod's high field and small size, the heat flux gradient scale lengths are relatively small, while the absolute densities

are the highest found in any of today's divertor tokamaks. The high densities yield high collisionalities, as well as relatively high values for $\lambda_n^{perp}/\lambda_{ni}$. In C-Mod the short neutral mean free path is dominated by charge exchange. More on the behavior of neutrals in C-Mod can be found in Ref. [9]. Most of the evaluations in Table I, as well as the SOL profiles discussed below, rely on measurements made using reciprocating probes [1,5,10,11,12,13], and much more information about conditions, scalings, and analyses can be found in those references.

II. a. Density and Temperature Profiles

The SOL profiles of temperature and density are crucial in setting divertor heat loads and particle pumping capability. Typical density and temperature profiles and their dependences upon core plasma density are shown in Fig. 2. They are shown for core densities increasing from $1x10^{20}$ m^{-3} to $2.6x10^{20}$ m^{-3} ($0.17 < n_e/n_{GW} < 0.45$). The density profiles show clearly the break in slope (discussed above) between the near-SOL, where the density falls rapidly with ρ, and the far-SOL, where a "shoulder" region of less strongly decaying or constant density exists. In the near-SOL λ_n^{perp} is typically ~4 mm. As the density is raised, the far-SOL density increases and the "shoulder" flattens, indicative of increased radial transport, increased ionization source, or both. Defining an "effective diffusion coefficient", $D_{eff}=\Gamma_{perp}/\nabla_{perp}n_e$, it is found that D_{eff} increases with radial distance into the near-SOL, reaching values as high as 10 m^2s^{-1} in the far-SOL [1]. Furthermore, it is found [1,6] that D_{eff} in the *near-SOL* scales $\sim\lambda_{ei}^{-1.7}$ or equivalently $\sim(\nu^*)^{1.7}$, as shown in Figure 3. The use of D_{eff} is not meant to imply that the transport is wholly or even dominantly diffusive, since, as discussed below, there is strong evidence that convective transport dominates in the far-SOL. Nonetheless, it is useful in characterizing the anomalous perpendicular particle transport in the near-SOL.

Alternatively, when the transport in the SOL is characterized by an "effective convection velocity", $v_{eff}=\Gamma_{perp}/n_e$, then it is found [14,15] that v_{eff} increases strongly with distance from the separatrix. This is not surprising given the observations regarding the cross-field profiles of D_{eff}. In addition, dimensionless-scaling experiments, comparing C-Mod, DIII-D, and JET, show that *in the far-SOL* v_{eff} appears to be independent of or weakly-dependent on the dimensionless plasma-physics quantities, ν^*, β, or ρ^* [14,15]. SOL profiles of v_{eff} from the three devices are shown in Fig. 4. All v_{eff}s have been scaled appropriately for size differences using a dimensionless scaling methodology [14,15]. The three C-Mod profiles are the same for both Fig. 4(a) and 4(b) and correspond to Greenwald fractions of 0.15, 0.25 and 0.36. The ranges of Greenwald fractions covered by the four DIII-D and the four JET discharges are 0.25 – 0.55 and 0.34 – 0.65 respectively. Because the far-SOL v_{eff} hardly varies for a wide range of densities, any dependence of v_{eff} on ν^* is weak. Any dependence on ρ^* and β is also weak, as demonstrated by scans of magnetic field and current [15]. The independence of the scaled v_{eff} in the far-SOL with respect to ν^* is quite different than the strong dependence of D_{eff} on ν^* in the near-SOL.

While the results of these dimensionless scaling comparisons show essentially the same far-SOL transport for each of the three machines, *there can be marked differences in SOL profile shapes*. In particular, the JET density profiles in the far-SOL tend to be steeper (less flat) than those of C-Mod. Thus, we believe that some of the variation in density profile shape (like that shown in Fig. 2a and that between machines) is due to variation in the SOL's opacity to neutrals. (JET's SOL is much more transparent to neutrals than C-Mod's.)In other words, the "shoulders" seen in C-Mod are created in part by ionization of recycling neutrals. Indeed, there is the potential for a positive

feedback between the far-SOL ion fluxes and the local ionization: local recycling of increased ion fluxes leads to higher neutral densities with accompanying local ionization, leading to higher local plasma densities, increased opacity to neutrals, higher outward ion fluxes, and so on….

In summary, we measure large levels of perpendicular particle transport in the near and far-SOL (as characterized by D_{eff} and v_{eff} respectively). In the near-SOL it scales strongly with ν^*, while in the far-SOL the transport appears not to depend on dimensionless quantities ν^*, β, or ρ^*.

Table I does not distinguish between SOL parameters in L-mode and in H-mode plasmas; the ranges indicated cover both conditions. With regard to L/H-mode differences, we note that the SOL flows may play a crucial role in the H-mode as a result of momentum coupling across the separatrix (see Sect. VI). Operationally, C-Mod plasmas typically respond to an L- to EDA H-mode transition with an increase in steady-state line-averaged density (by about a factor of 2 or less). The pressure gradient scale lengths in the *near-SOL* decrease significantly (also by a factor of ~2) [11], as do values for D_{eff} [1], implying that the H-mode edge transport barrier extends somewhat into the SOL. However the far-SOL is relatively unaffected, with the profiles there retaining their L-mode values and L-mode scaling [11]. Thus, neither v_{eff} nor the perpendicular particle flux in the far-SOL, $\Gamma_{perp}^{far\text{-}SOL}$, appears to depend on confinement mode.

II. b. "Main-Chamber Recycling"

The tendency for rapid cross-field transport in the far-SOL has potentially important consequences for reactor operation, a subject in which C-Mod has made significant

contributions. One of the primary functions of the divertor is to remove, as much as possible, the plasma-wall interaction physics (e.g., the high heat fluxes and impurity generation from particle impact) away from closed magnetic flux surfaces, thus minimizing the impurity levels in the confined plasma. However, enhanced cross-field particle transport in the far-SOL can potentially reduce the effectiveness of the particle-handling function of the divertor (including He "ash" removal) by preferentially increasing the particle fluxes to and refueling from the walls facing the confined plasma, i.e. the *main-chamber walls*. One might expect this effect to be particularly manifest in divertors that are shaped for optimum heat-flux handling – an optimization that is required in ITER and power-producing reactors. The reason for this expectation is: As shown in Fig. 1, Alcator C-Mod employs a "vertical-plate geometry" divertor. This geometry spreads the heat flux over a large area and enables the divertor target material in C-Mod (molybdenum) to avoid melting. In order to keep the length of the "vertical plate" from being too large and occupying too much expensive space, the location of the *divertor throat*, which is defined here as the transition point from a 'vertical plate' orientation to a more horizontal inclination, is placed only a few heat-flux e-folding distances away from the LCFS (see Fig. 1). Thus, for C-Mod, the *main-chamber wall* surfaces include the nearly-horizontal surfaces just above the divertor throat as well as the vacuum vessel wall and the main-chamber limiters.

Indeed, the first systematic investigation of plasma recycling light in the main-chamber scrape-off layer of Alcator C-Mod uncovered a surprisingly high level of main-chamber interaction [16]; in medium and high-density discharges, the number of ionizations per second in the main chamber was found to exceed by more than an order of magnitude the rate at which ions were lost to the divertor volume by parallel flow from the main-chamber; thus the neutrals

corresponding to this divertor loss that might return to the main chamber could not explain the high neutral densities there. The implication was that plasma in the main-chamber SOL recycles primarily via interaction with the main-chamber surfaces rather than through interaction (i.e. an exchange of plasma and neutrals) with the divertor volume. Further investigations [1,6,17,18], including direct measurements of particle fluxes onto main-chamber limiter surfaces and analysis of the neutral 'leakage' from divertor to main-chamber regions, confirmed the initial observations. Moreover, two principal ingredients consistently emerged as responsible for the observed high level of main-chamber recycling: (i) the existence of a rapid cross-field particle transport mechanism in the far-SOL and (ii) the small width of the divertor throat (e.g., ~2 power e-folding widths from the LCFS). As stated in Ref. [1], the former observation has become a potential concern for reactor designs: "This fundamental characteristic of main-chamber SOL transport is troublesome: there may be no practical way to design an "ideal" divertor for Alcator C-Mod that would accommodate the width of the particle flux profile in the main-chamber SOL. Similar to Alcator C-Mod, fusion reactors will employ a tightly baffled, heat flux optimized divertor geometry and operate with wall surfaces that are fully saturated (i.e. with a particle recycling coefficient of unity). Thus, the physics behind this regime of main-chamber recycling needs to be understood in a way that can be extrapolated to reactor conditions."

The identification of a strong "main-chamber-recycling" regime on C-Mod was an important development that helped to prompt the community to search for a common framework with which to compare main-chamber recycling observations from different machines [19]. A goal has been to build a physics-based understanding that can be extrapolated to reactor conditions.

We note that among the world's diverted tokamaks there appears to be a continuum of behaviors, spanning conditions where most of the ion loss is to the "main-chamber" to where most of the loss is to the "divertor-targets" [19,20]. The reasons for the differences need to be understood and are presently under investigation. However, sometimes these differences have been thought to be evidence that the "main-chamber recycling" phenomenon is somehow unique and specific to C-Mod and therefore perhaps not of significant consequence to a reactor. In light of this potential ambiguity, we feel that it is necessary to discuss some of the commonalities and differences among experiments in an attempt to clarify the present state of affairs.

First, it is important to point out that Alcator C-Mod was not the first machine in which "shoulders" in SOL density profiles were observed, nor were C-Mod researchers the first to note that the shoulders implied large levels of cross-field transport there (much larger than Bohm-like transport) [21,22,23]. Indeed, "shoulders" and a two-zone SOL structure have been observed on most tokamaks, ASDEX[21,24,25], ASDEX-Upgrade[22,23], TEXT-U[26], DIII-D[27,28,29,30], JT-60U[31], JET[32], TEXTOR[33], and TCV[34] and are common features. Therefore, it appears that plasma turbulence in the SOL, and the rapid transport mechanism associated with it in the far-SOL in particular (discussed below in Section III), are features that are truly universal among tokamaks. Also the turbulence in the SOL (discussed in Section III) appears to have many characteristics that are universal to tokamaks. In sharp contrast, the first-wall and divertor geometry is *not* universal to tokamaks – the distance from the LCFS to the first wall or to the *divertor throat* varies greatly. As a result, there are many different potential definitions of the terms "main chamber" and "divertor throat" especially in machines with more

"open" divertors [23]. These differences by themselves can lead to large variations in the reported "main-chamber recycling flux".

A useful unifying concept in the discussion of main-chamber recycling is the idea that each magnetic flux surface in the SOL effectively defines a surface through which the particles may pass through only by cross-field transport. The most important flux surface (in the present context) is the one that intercepts the main-chamber wall surface which is closest, in a flux-surface mapping sense, to the LCFS, be it a limiter or the material surface above the entrance to the divertor (e.g., the divertor throat – see Fig. 1). For C-Mod we define the plasma flux passing through this surface to be the flux to the main-chamber surfaces. The resultant neutrals due to the recycling of this ion flux return through the same "window-pane". In the special case where neutral ionization can be neglected outside this flux surface (compared to transport), the particle flux through it may be measured as the ion flux to wall-mounted Langmuir probes. This concept was used as the basis for measurement of the radial ion flux passing between two limiters (the limiter recycling fluxes) in C-Mod [1,35] and was subsequently generalized to toroidally-symmetric recycling surfaces [19]. It is now known as the "window-frame/window-pane" technique. The "window-pane" concept also helps illustrate two important points: (i) the main-chamber recycling flux, as defined by the flux crossing the "window-pane" associated with the nearest main-chamber surface (*the divertor throat for C-Mod*) is set by the cross-field transport on that flux surface, and consequently (ii) the separation distances between the "window-pane" and other *secondary* main-chamber surfaces (local limiters, walls, etc) do not affect the magnitude of the so-defined main-chamber recycling flux (barring some non-linear effect on plasma transport due to recycling). These separation distances affect only the spatial distribution

of the flux to these secondary surfaces. (Such a redistribution could, for example, change impurity sources and levels in the core plasma and/or core fueling efficiencies.) Therefore, even if the gaps to secondary surfaces were made very large, the main chamber recycling flux would persist at the same level.

Seen in this context then, a unifying perspective on "main-chamber recycling" can be stated: it is the rapid-transport physics of the far-SOL (which appears to be universal among tokamaks) combined with the machine-specific definition of the main-chamber "window-pane" that determines the relative amount of "main-chamber-" versus "divertor-recycling" that is observed. For heat-flux optimized divertors (such as C-Mod's), where the divertor throat must be placed a few heat-flux e-folding lengths from the LCFS, the main-chamber fluxes may be especially high – a direct consequence of the far-SOL transport physics. This view appropriately puts the emphasis on the understanding the underlying transport physics (such that it can be properly simulated in 2-D transport codes, for example), and not whether the dominant SOL ion loss in a given tokamak is seen to be to the "main-chamber" or to the divertor, since this depends on specific location of the "window-pane".

Finally, before leaving the discussion of "main-chamber-recycling", we collect several important questions that need to be dealt with in the future: 1) What determines the boundary between near- and far-SOL? 2) How does its location scale (especially with regard to ITER)? 3) How do we predict the SOL density profiles, in particular "shoulders" in the far-SOL? The answers to these questions will require understanding the dominant transport mechanisms in both SOL regions, and the answer to question 3, as discussed earlier, will probably require understanding

the role of neutrals. In addition, if we really believe that "blobs" (see Section III) originate in the strong gradient region of the near-SOL, then we may need to study the far SOL as an example of non-local transport, understanding how the far-SOL characteristics depend on the near-SOL, or not.

II. c. Neutral Pressure in the SOL

Main-chamber recycling and the anomalous perpendicular transport that gives rise to it are the dominant factors in determining the main chamber or "midplane" neutral pressure in C-Mod, with gas leakage from the divertor contributing only 10-30% [18]. Because in C-Mod the midplane pressure is related to characteristics of the SOL and not the divertor, the scaling of the neutral pressure and the small response of the neutral pressure to L- and H-mode confinement are worthy of note here (see also Ref. [9]). In C-Mod the midplane pressure depends strongly on plasma density, scaling approximately as $n_e^{3\text{-}4}$ [1,8]. This strong scaling with plasma density is seen in both L- and H-mode. The midplane pressure does not change significantly at or after a confinement mode transition. This is due to the fact that the far-SOL perpendicular ion fluxes are essentially unaffected by the confinement mode. In the near-SOL the increase in density gradient is approximately compensated by the decrease in the effective transport coefficient. However for the same neutral pressure, since the line averaged density is ~2x greater in EDA H-mode than in L-mode, the scaling of pressure with *line averaged density* is offset for H-mode relative to L-mode [18].

II. d. Heat Transport in the SOL

We note first that the peak parallel heat flux in the SOL can be quite large, ≤ 500 MW m^{-2}, approaching that expected for ITER. Secondly, the idealized-divertor paradigm of parallel conduction dominating energy transport is still valid in C-Mod's *near-SOL*, where almost all of the power flows as long as n_{sep}/n_{GW} does not exceed ~0.4 [6]. (Those cases with $n_{sep}/n_{GW} > 0.4$ will be discussed in Sect. IV.) In the far-SOL the power convected perpendicular to B is larger than that conducted parallel under almost all C-Mod conditions, although the power flowing in this region is relatively small. As is evident in Fig. 2b, the temperature and the temperature gradients near the separatrix vary little as n_e is increased (as long as it remains somewhat below ~$0.7n_{GW}$, see Sect. IV). The narrow variation of the separatrix temperature, $T_e(\rho=0)$, is consistent with the prediction from simple modeling that $T_e(\rho=0)$ is set by parallel heat conduction and has a very weak dependence upon power flowing into the SOL, i.e. $T_e(\rho=0) \sim P_{SOL}^{2/7}$. The temperature gradient scale lengths near the separatrix are typically ~4-10 mm in L-mode and 2-6 mm in H-mode, gradually increasing as a function of ρ. In the region beyond the limiter shadow, the temperature is almost always in the range 5–10 eV with a small gradient.

III. Edge/SOL turbulence

The time-averaged SOL characteristics cannot at the present time be determined from a first-principles physics model. The large values of inferred D_{eff} or v_{eff} show clearly that the cross-field transport in the C-Mod SOL is anomalous, set by the properties of plasma turbulence. This section examines the evidence for and the characteristics of the dominant turbulence in the C-Mod SOL.

The size- and time-scales of the turbulence in C-Mod were first apparent in fluctuations of both probe and optical signals from the SOL. Fluctuations on the ion-saturation-currents (I_{sat}) and in the D_α emissions show strong intermittency in the far-SOL, with distributions in the fluctuation magnitudes that are skewed toward larger magnitude fluctuations. The relative fluctuation magnitude and the skewness of the fluctuation distributions increase with ρ and with main plasma density. These observations are illustrated in Figure 5. The time-scale for the fluctuations is in the 1-50μs range. Initially, fluctuations in $V_{floating}$ and I_{sat} from the scanning probe were analyzed, leading to the following observations: "At low [plasma] densities, the fluctuations are close to Gaussian noise with a very low level of intermittency. At high density, the intermittency, correlation time, and long-range dependence significantly increase. The … analysis seems to indicate the presence of bloblike … structures … correlated over long times. Similar structures are present in the turbulence-induced fluxes. These structures may be responsible for the large cross-field transport that plays a dominant role in the main chamber recycling in Alcator C-Mod." [36] It was also concluded in Ref. [36] that much of the far-SOL transport is driven by large but relatively infrequent fluctuations; events with a magnitude ~5 times the average can account for ~50% of the total particle transport.

Experiments to image the "bloblike structures" were subsequently undertaken using "Gas-Puff-Imaging" in D_α and He line emission [37,38,39,40,41,42,43]. The technique relies on the fact that the imagable emission fluctuations result from local fluctuations in density and temperature. Indeed blobs were found. Imaging in the vertical-toroidal plane showed them to be fluctuations with a filamentary structure, aligned with the local field and with $k_{\|} << k_{pol}$. When these filaments

are viewed in a vertical-radial plane, along chords parallel to the local field, they appear as blobs with a characteristic size of ~1 cm in both poloidal and radial dimension in the far-SOL. As an example of the birth and movement of blobs, twelve consecutive frames of a GPI movie are shown in Fig. 6. From multi-frame movies like these, it is evident that generation and propagation of these turbulent structures are responsible for the large amplitude fluctuations on the probes' $I_{sat}/V_{floating}$ signals and on the optical emission signals, as they sweep past the observation locations. Movies [42](with up to 300 sequential frames) utilizing GPI, as well as arrays of localized views that have been coupled to filtered diodes [37], have yielded a wealth of information characterizing the blobs and their dynamics [38,39,42,43,44,45]. In discharges *not* close to the density limit the blobs are observed to be born in the near-SOL and to propagate radially outward and poloidally at speeds up to ~1 km/s. This typical case is illustrated in Figure 6. A summary of some of the blob characteristics is presented in Table II.

property	value	Comment/Ref.
Radial correlation length	7-15 mm	Characteristic radial size [38,39]
Poloidal correlation length	6-10 mm	Characteristic poloidial size [38,39]
$k_{pol}\,\rho_s$	~0.03	[39]
Auto-correlation time	1-50 μs	Characteristic life time [37,38,39]
Radial speed (outward)	<1.5 km/s	[43,44]
Poloidal speed	<1 km/s	[43,44]

Table II. *Some of the properties of blobs in L-mode plasmas, as measured using GPI optical diagnostics and probes.*

A preliminary study of the differences, if any, in the blob characteristics between L- and H-mode has been accomplished in C-Mod plasmas [45]. These turbulent structures and their dynamics are qualitatively similar in both confinement modes. Quantitatively, it is found that their perpendicular extent is somewhat smaller in ELMfree H-mode (~0.4 cm compared to 0.4-1 cm in L-Mode), while their occurrence frequency is similar. A difference is seen in the *magnitude* of these turbulent fluctuations in the far-SOL, with blobs in H-mode showing a factor of 2-3 times smaller perturbation there than L-mode.

Recent advances in the numerical modeling of turbulence have allowed detailed comparisons with the experimental observations. The simulation models used for these comparisons [46,47,48,49] are non-linear drift-ballooning codes that solve the Braginskii fluid equations for electrons and ions in a 3-D geometry (in the C-Mod SOL $\lambda_{ei}/L_{\|}<0.1$). They included diamagnetic, magnetic shear, and toroidal curvature effects. In the simulations the time-averaged profiles were fixed to be the experimental ones. A number of quantities calculated in the simulation were compared directly with the experiment: simulation and experimental time-averaged particle fluxes were found to agree to within about a factor of two and a good match between experiment and simulation was found for the k_{pol} spectra ($2 < k_{pol} < 15$ cm^{-1}), as well as for the autocorrelation times vs. ρ. The simulations identify the resistive ballooning instability as the dominant linear instability [39]. However, there are still many areas where the experiment/simulation comparisons are deficient, so they are best considered at the present time as promising initial attempts. A "first principles" understanding for the origin and evolution dynamics of the blobs is still being sought. Such an understanding could also be used to generate time-averaged profiles that could be compared to those measured experimentally.

IV. Relationship between the SOL and the Density Limit

The Greenwald density limit scaling [$n_{GW}(x10^{20}\ m^{-3}) = I_p(MA)/\pi a(m)^2$] was derived from a relatively small data set [50] well before C-Mod was commissioned. Two of the striking features of the limit scaling are its relative simplicity and its robustness [2]. It has proven to be approximately valid across a wide range of confinement configurations, shapes, and aspect ratios, and indeed Alcator C-Mod follows this scaling [6]. Thus it is generally assumed that there is a common physics basis for the limit, independent of poorly controlled variables like impurity content and wall condition. Furthermore, although the scaling is remarkably robust, it does not hold in cases with strongly peaked density profiles. These and other factors have resulted in C-Mod researchers proposing the reasonable hypothesis that *edge transport* plays a crucial role in the limit [1,2,6]. Before summarizing that research, we note the importance of such a density limit. As discussed in detail in [2], not only does it constrain desired high-density reactor operation, but it is also clearly coupled to the density at which H-mode is possible. The density limit for high quality H-mode confinement is seen to scale approximately as ~0.7 n_{GW}[2].

Research on the density limit in C-Mod supports the hypothesis that the turbulent, convective transport observed in the far (outboard) SOL encroaches on the closed flux surfaces near the density limit, convecting both particles and heat to the open field lines in the SOL with the ultimate result that the plasma column cannot be sustained. Although this hypothesis is by no means proven, it is supported by the following observations: It is consistent with the near-SOL transport scaling strongly with collisionality, ν^* (see Fig. 3). It is also consistent with the

analyses of the perpendicular and parallel heat and particle transport and their dependences on n/n_{GW}, discussed in detail in Ref. [6] and illustrated in Fig. 7. Fig. 7 shows the scaling of the SOL power balance with normalized density. The power conducted to the divertor is *exceeded* by the power convected across the separatrix out to the main-chamber limiters for $n/n_{GW} > 0.4$. Additionally, radially resolved estimates of the parallel conducted power and perpendicular convected power show that convection exceeds conduction over the entire SOL for $n/n_{GW} > 0.4$. Furthermore as the limit is approached, we observe that the intermittent, blob transport, typically found in the far-SOL, *does* move toward and inside the separatrix to the closed flux surfaces. This is seen both by the probes [6] and by the optical diagnostics [39,45]. For $n/n_{GW}>0.6$, some blobs are born on *closed* flux surfaces, as can be seen in Fig. 8, in contrast to what is observed in discharges with lower density, when blob generation typically occurs only outside the separatrix. Compare the blob generation location in Fig. 8 (in a discharge that approaches the density limit) with that shown in Fig. 6 (in a discharge well away from the limit). Other, more quantitative, measures of the turbulence indicate that the turbulence and transport characteristics of the far-SOL move radially inward. As illustrated in Fig. 9, the normalized emission fluctuation profile shifts to smaller ρ. The region of large skewness in the fluctuation distributions (both for GPI emission and I_{sat}) also shifts inward. Fig. 9 also shows the T_e profiles at medium and high normalized density. At $n/n_{GW} = 0.8$ the parallel heat conduction losses no longer regulate the magnitude or shape of the T_e profile anywhere in the SOL. Of course these results do not reveal reasons for the simplicity and robustness of the density limit scaling. A relatively strong dependence of the near-SOL's effective diffusion coefficient upon plasma current, the key dependence in the limit, exists through the connection length that is contained in ν^* ($=L_{\parallel}/\lambda_{ei}$).

Although this relates the density, current, and transport in a sense consistent with the limit scaling, considerably more work is needed before such a simple scaling is explained.

V. Differences between Inboard and Outboard SOL

Plasma conditions in the SOL vary strongly as a function of poloidal location. This is not surprising given that the outboard (low-field side) SOL is in a "bad" curvature region, that inboard (high-field side) is a "good" curvature region, and the existence of magnetic X-points that tend to isolate the two regions. C-Mod has provided some of the first measurements of the inboard SOL, primarily because of innovative diagnostics that provide access to this region. As with the outboard diagnostics, measurements are made by a reciprocating probe [51,52] (in this case mounted on the central column) and a radial array of optical views, looking parallel to the local field and utilizing GPI for emission localization [39,53]. The main differences between the inboard and outboard SOL are: 1) the turbulence level is much lower on the inboard side; 2) the inboard SOL properties (e.g. profiles and flows) are much more sensitive to the magnetic topology, and 3) the characteristics of the time-averaged parallel plasma flows are different. We observe that the normalized fluctuation levels of the GPI emission are approximately a factor of ten smaller than those measured simultaneously *on the same flux surfaces* at the outboard midplane [39]. The shape of the frequency spectra of the emission fluctuations is quite different as well. Inboard and outboard probe measurements of I_{sat}^{RMS}/I_{sat} yield results similar to those from the optical diagnostics, where the inboard side reduction is a factor of ~3-10 [51]. The *absolute* RMS level of I_{sat} fluctuations is also significantly lower (~x3) on the inboard side.

It is also observed that the inboard SOL characteristics depend sensitively upon the magnetic topology. This was seen initially [54] as an absence of plasma on the inboard field lines isolated from the outboard plasma by *both* primary and secondary separatrices. (The secondary separatrix is that flux surface defined by the second, non-dominant X-point or by the intersection with a mechanical structure). Other work [51] has revealed the details of this sensitivity on topology. The inboard/outboard pressure profiles are typically constant on the "common flux" surfaces between the separatrices, but on inboard SOL flux surfaces that are magnetically isolated from the outboard side there is very little plasma. As will be discussed in more detail in Sect. VI, the inboard/outboard plasma flows are also quite different [51]. Parallel flows in the inboard SOL are directed toward the dominant X-point with magnitudes approaching Mach 1, i.e. $|M_{||}|=|v_{||}|/c_s \sim 1$, where c_s is the local sound speed and $v_{||}$ is the parallel flow velocity. Outboard flows are smaller, typically with $0 \leq |M_{||}| < 0.4$, and dependent upon poloidal location, distance from the separatrix, and density. The surprising picture that has emerged, as concluded in Ref. [51], is that probe "data from different magnetic topologies (lower X-point, upper X-point, double-null) indicate that a ballooning-like component of the cross-field plasma transport is the underlying cause for the strong parallel flow [on the inboard side]—in single-null topologies, plasma exists on the high-field side SOL *principally because it flows along field lines from the low-field side*." As discussed previously, the SOL plasma on the outboard side is present primarily because of ballooning-like/curvature-driven cross-field transport.

VI. Flows in the SOL

The importance of understanding SOL flows derives from its possible impact on impurity transport, plasma fueling, divertor plasma asymmetries, and the effect they might have on the core plasma, in particular regarding momentum coupling. Plasma flow in the SOL is complex mainly because there exist so many mechanisms that can drive flow. Parallel flow can be a result of ionization imbalances, Pfirsch-Schluter flows, and poloidal transport asymmetries, and toroidal rotation. Perpendicular flow consists of ExB and diamagnetic contributions. Interest in and the study of plasma flow has had a long history at C-Mod. Initial work [11] found that parallel flows above the outer divertor were directed towards or away from the divertor entrance, depending on the plasma current and toroidal magnetic field direction. The sometimes "reversed flows" (away from the divertor) appeared to circulate the plasma poloidally, suggesting that an asymmetry in divertor ionization may be partly responsible. There have also been spectroscopic studies of neutral (D_0) [55,56] and ion (He+) flow [56]. More recently work has illuminated a strong dependence of the parallel flow magnitude and direction on magnetic topology, as well as a flow momentum coupling between the core and SOL [51]. This work has synthesized a number of heretofore unrelated observations into an intriguing picture of transport-driven SOL flows, SOL-core plasma momentum coupling, and L-H mode transition physics. The rest of this summary focuses on this recent work.

Using probe diagnostics of inboard and outboard SOL, as well as measurement of core toroidal rotation, a complex picture of polodially asymmetric transport, edge flows and core toroidal rotation emerges. As stated in Ref. [51], the work "has revealed a rich interplay among anomalous cross-field transport, strong plasma flow along magnetic field lines, magnetic topology and toroidal rotation in the edge plasma. In particular, remarkably rapid plasma flows

parallel to magnetic field lines are observed in the high-field SOL." Shown in Fig. 10a are the SOL flow velocities as measured at ρ=2 and 1 mm on the inboard and outboard sides, respectively, in Ohmic L-mode plasmas. *Topology-dependent* parallel flows close to Mach 1 are observed in the inboard SOL, directed toward the dominant X-point. (In Fig. 10 and hereafter in the text, the + flow direction is co-current, while – flow is counter-current.) The origin of the strong parallel flows in the inboard SOL has been shown to be a result of a strong ballooning-like component of the cross-field transport. Some of the strong evidence for the large poloidal asymmetry in the turbulent transport has already been discussed in Section V. With reference to Fig. 11a, a preponderance of radial particle flux on the outboard side leads to parallel flow arising in order to re-symmeterize the resulting poloidal pressure variation in the SOL. With an X-point present, one of the flow paths (via the top or bottom) to the inboard SOL is blocked, so Lower Single Null (LSN) exhibit strong parallel flow in the inboard SOL in the co-current direction, while the inboard SOL flow in Upper Single Null (USN) plasmas is seen to be strongly counter-current, as shown schematically in Fig. 11a. While the SOL flow directions shown in the top two panels of Fig. 10a are fully consistent with this picture, it should be noted that the flow analysis is based on a much larger data set than that of Fig. 10a [51]. Data-constrained modeling of the asymmetric ballooning-like transport shows that the SOL can possess *by this mechanism* a net volume-averaged toroidal momentum in the measured, topology-dependent direction. The response of the core plasma to the boundary condition imposed by the strong SOL parallel flows was investigated, with the result that the SOL flows do appear to couple to the confined plasma, thus affecting the toroidal rotation of the plasma as a whole (at least in Ohmic L-mode plasmas, since once the H-mode is achieved, the SOL flows do not appear to play a dominant role in setting the rotation of the core plasma).

In fact, the core rotation velocities (shown in the third panel of Fig. 10a) and the toroidal projection of the outboard SOL flow velocities are linearly related (Fig. 10b), consistent with a momentum coupling across the separatrix in these L-mode plasmas. Indeed, the strong negative (counter-current) inboard SOL flows in USN appear to enhance the "intrinsic" negative (counter-current) core rotation observed in the DN case, making it more negative. Additionally, the positive (co-current) SOL flows in LSN appear to resist the "intrinsic" negative core rotation making it significantly less negative than that observed in DN. The mechanism for the implied SOL-core momentum coupling is as yet unknown. Assuming the implied existence of core/SOL momentum coupling, then once the core plasma is rotating, this can act back on the SOL, presumably by affecting the SOL radial electric field and providing an incremental change in the toroidal rotation component for the flows measured in SOL. This mechanism is illustrated in Fig. 11b. Using topology changes to separate out different components of the measured parallel flows, the experiments showed precisely the expected tendencies, i.e. in LSN plasmas stronger co-current rotation is measured in the core and a more positive E_r is measured in the SOL, while weaker co-current rotation and a less positive E_r are measured for USN. (The possibility of a toroidal rotation component present in the measured parallel SOL flow was first raised in Ref. [57], where magnetic topology changes were also employed to elucidate the picture.)

Finally, this research makes an important connection with a long-standing, universal puzzle about the influence on the L-H transition power threshold of the X-point location relative to the B x ∇B direction. On diverted tokamaks the power threshold has been found to be significantly lower if the B x ∇B direction "points toward" the dominant X-point. Or, stated in a manner more relevant to the picture presented here, if the current and magnetic field directions and X-point

location are such that the high-field-side SOL flow is strongly co-current, the L-H power threshold is significantly lower. In addition to the observations of topology-dependent SOL and core flows, three other facts are relevant to the hypothesis that purports to solve this puzzle on C-Mod: 1) as seen in Fig. 10b, Ohmic L-mode plasmas have a central rotation that is counter-current (with a magnitude that is topology-dependent), 2) it is observed in all C-Mod topologies (LSN, DN, and USN) that the L–H transition occurs when a zero or slightly co-current central plasma rotation is achieved, and 3) in C-Mod higher input power (which imparts no momentum to the plasma) tends, via an as yet unknown mechanism, to spin the plasma in the co-current direction through an increase in stored plasma energy [58]. Thus in an "unfavorable" geometry, where the SOL flow boundary condition *impedes* co-current plasma rotation, more power is require to spin the plasma up to the threshold co-current rotation [51].

VII. Summary

Research on Alcator C-Mod has made significant contributions to the understanding and characterization of the scrape-off-layer plasma. Perhaps most importantly, work on C-Mod has entailed extensive measurements of transport properties in the SOL, has focused attention on the differences in transport in the near- and far-SOL, and has studied the consequences of both the transport and the near/far-SOL differences. Indeed, perpendicular transport of ions at the outboard, "bad" curvature side of the plasma can dominate parallel transport, leading to large radial ion convective fluxes in the outboard SOL and strong flows in the SOL globally. The turbulent transport responsible for this has been characterized and found to be associated with the generation and radial propagation of field-aligned plasma filaments – blobs - that convect

particles and heat from hotter denser regions to and through the far-SOL. In C-Mod this physics results in a "main-chamber recycling" regime, a condition where there is significantly more loss of plasma ions to main-chamber surfaces than loss through the divertor throat. This condition dominates the determination of the main chamber pressures, which are only weakly dependent upon the divertor pressures and divertor-to-chamber gas conductances. While it is recognized that the magnitude of the main-chamber recycling fluxes depends on both the location of the flux surface that intercepts the closest wall surface (defining the "main-chamber window-pane") and the cross-field particle transport at that surface, it is the latter quantity that is fundamentally important and immutable for a reactor design. In reactors that require the divertor surface to be optimized solely for the purpose of power flux handling (as in C-Mod), this will lead to an irreducible flux of main-chamber wall interaction. Moreover, experiments in C-Mod indicate that the strong radial convective transport, typically restricted to the far-SOL, moves inward to closed flux surfaces as the density limit is approached and may therefore play a role in defining that limit. Novel diagnostics accessing the high-field-side SOL on C-Mod have enabled the detailed characterization of the strong inboard/outboard asymmetry in the SOL plasma –both in its time-averaged parameters and in its turbulence. The asymmetric transport is seen to drive strong parallel flows in the high-field-side SOL. There is strong evidence for momentum coupling across the separatrix to the core plasma. This coupling and drive has numerous important consequences, including a possible key role in the physics of the L-to-H-mode confinement transition.

Acknowledgements

The authors thank the Alcator C-Mod operations group for expertly providing the discharges used in these studies. This work is supported at MIT by DoE Contract No. DE-FC02-99ER5412.

Figure Captions

Fig. 1. *Cross-section of Alcator C-Mod. The LCFS is indicated by the thick black line; flux surfaces in the SOL are indicated by green lines. The lower, baffled divertor has had two shapes for its inner structure – a more tightly baffled shape (shown in gray) in existence through 2002, and a vertical cross-section inner divertor since that time (overlaid in black). The opening to the divertor throat defines the main-chamber "window-pane" flux surface (thick-dashed line – See Sect. II.b). Note that the gaps to both the inner-wall and outboard limiter are typically* external *to this "window-pane" flux surface. Also shown are the locations of some of the key SOL diagnostics – the probes and the regions imaged by "gas-puff-imaging" (GPI) optical diagnostics. The outboard diamond is the view of the fast camera; the dots are the views of the various fiber-based arrays (not to scale).*

Fig. 2. *SOL density profiles (a) and temperature profiles (b) vs. core density. The location of the outboard limiter is indicated by the pink stripe. From [18].*

Fig. 3. *Results of correlating D_{eff} at ρ=2 mm with 2 sets of regressors: (a) T_e and ν^* and (b) ν^* alone. The regressions include 64 data samples, obtained in discharges in the parameter ranges: $0.6<I_p<1.0$MA, $4<B_T<6$T, $0.8x10^{20}<n_e<2.5x10^{20}m^{-3}$. From [1].*

Fig. 4. *(a) Profiles for the SOL values of v_{eff} comparing C-Mod and DIII-D at different values of n/n_{GW} (see text); and (b) comparing C-Mod and JET. The values are scaled appropriately for the size differences among the three machines. From Ref. [14].*

Fig. 5. *Panels on left: time snapshots of $I_{sat}/<I_{sat}>$ at different locations (as indicated by the range in ρ) as the probe traverses the outboard SOL. (Note that the time axis is relative since each snapshot is acquired at a slightly different time in the probes trajectory.) The characteristic e-folding times (τ_{AC}) of the auto correlation functions at the different locations are given at the right. Panels on the right: Probability distribution functions (PDF) of fluctuations on the GPI Dα light signal originating from the indicated ρ positions and showing the increase in 3rd moment (skewness) and 4th moment (kurtosis) of the PDF with increasing ρ. From [6].*

Fig. 6. *Sequences of 12 experimental images taken at a 250 kHz frame rate, showing the typical space and time evolution of blobs (developed blobs are circled by ovals). The red line is the LCFS; the white line is the toroidal projection of the outboard limiter. The images are D_α emission after D_2 has been puffed at the outboard nozzle, located at the extreme right of the image. Compare the blob generation region, typically at or outside the separatrix as shown here, with that shown in Fig. 8.*

Fig. 7. *Power balance of the SOL vs. normalized density n/n_{GW} for Ohmic L-mode plasmas.* P_{sol} *is the power flowing into the SOL based on input power minus core radiation.* $Q_{cond}(0)$ *is power conducted along field lines to the divertor. P_{lim} is power convected across a flux surface ~5 mm beyond the shadow of the main-chamber limiters.* $Q_{conv}(0)$ *is power convected across the separatrix based on $A_{LCFS}5T_e\Gamma_{perp}$. From [6].*

Fig. 8. *Sequences of six experimental images taken at a 250 kHz frame rate, showing space and time evolution of a blob in a plasma with n/n_{GW}=0.7. In these density limit cases blobs are seen to originate inside the LCFS. The red line is the LCFS; the black-white line is the toroidal projection of the outboard limiter. The images are emission of the 667 nm HeI line after He has been puffed at the outboard nozzle, located at the extreme right of the image. From [39].*

Fig. 9. *Radial profiles of T_e and normalized emission fluctuations, I^{RMS}/I_{ave},, at two values of n/n_{GW}, 0.33 (black) and 0.8 (gray). The emission fluctuations are in HeI. Near the density limit, blobs are seen inside the separatrix (Fig. 8). From [45].*

Fig. 10. *(a) Toroidal flow velocities as a function of magnetic flux balance between upper and lower X-point in otherwise identical discharges. The first two panels show the SOL velocities at the inboard midplane (on a field line that maps to ρ=2 mm) and at an outboard, Z=10 cm location (on a field line that maps to ρ=1 mm). The third panel shows the core toroidal rotation from spectroscopy. A positive (negative) distance between separatrices indicates a dominant upper (lower) null, and a positive (negative) velocity indicates a co- (counter-) current direction. (b) Measured relation between core toroidal rotation velocity and toroidal component of the || flow at the outboard location. The fitted dashed line has a slope of 1.5. From [51].*

Fig. 11. *(a) Poloidally asymmetric, ballooning-like transport leads to a net volume-averaged SOL plasma momentum, co- or counter-current directed, depending on X-point location. $V_{||\phi}$ is the toroidal component of the parallel flow. (b) The core plasma can react to this boundary condition with a positive (negative) increment in the co-current rotation, ΔV_ϕ, when $B \times \nabla B$ is towards (away from) the X-point. Correspondingly, incremental toroidal rotation in the SOL, $\Delta E_r \times B_\theta$, is influenced by core momentum coupled back into the SOL, becoming more (less) co-current through more (less) positive incremental changes in ΔE_r. From [51].*

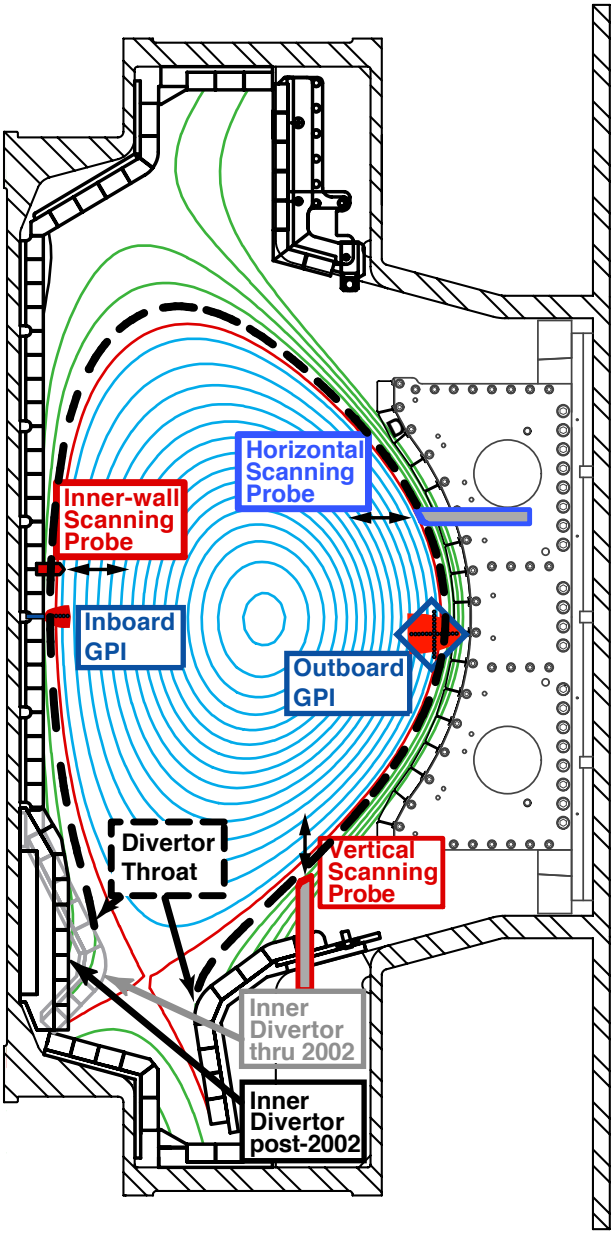
Horizontal
Scanning
Probe
Inner-wall
Scanning
Probe
Inboard
GPI
Outboard
GPI
Divertor
Throat
Vertical
Scanning
Probe
Inner
Divertor
thru 2002
Inner
Divertor
post-2002

Figure 1

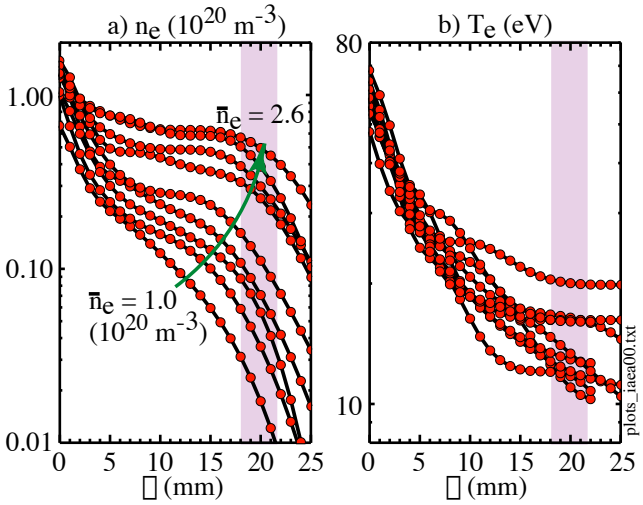
a) n_e (10^{20} m^{-3})
b) T_e (eV)
1.00
0.10
0.01
80
10
$\bar{n}_e$ = 2.6
$\bar{n}_e$ = 1.0
(10^{20} m^{-3})
0 5 10 15 20 25
□ (mm)
0 5 10 15 20 25
□ (mm)
plots_iaea00.txt

Figure 2

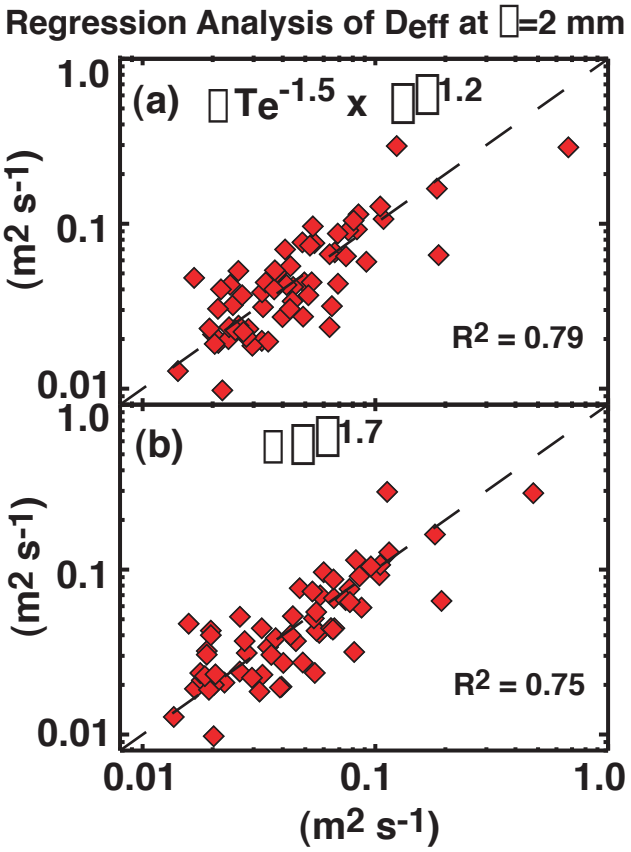
Regression Analysis of Deff at =2 mm
(a) Te-1.5 x 1.2
R2 = 0.79
(b) 1.7
R2 = 0.75
1.0
0.1
0.01
(m2 s-1)
0.01
0.1
1.0
(m2 s-1)

Figure 3

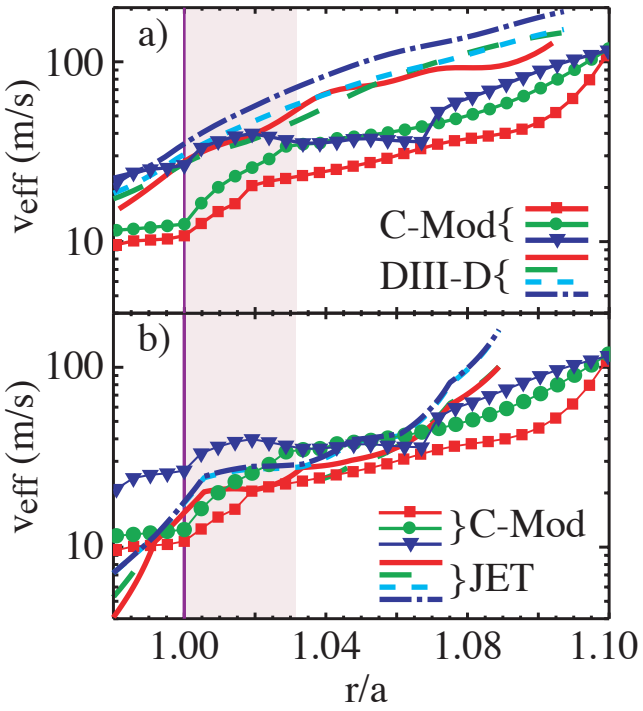

Figure 4

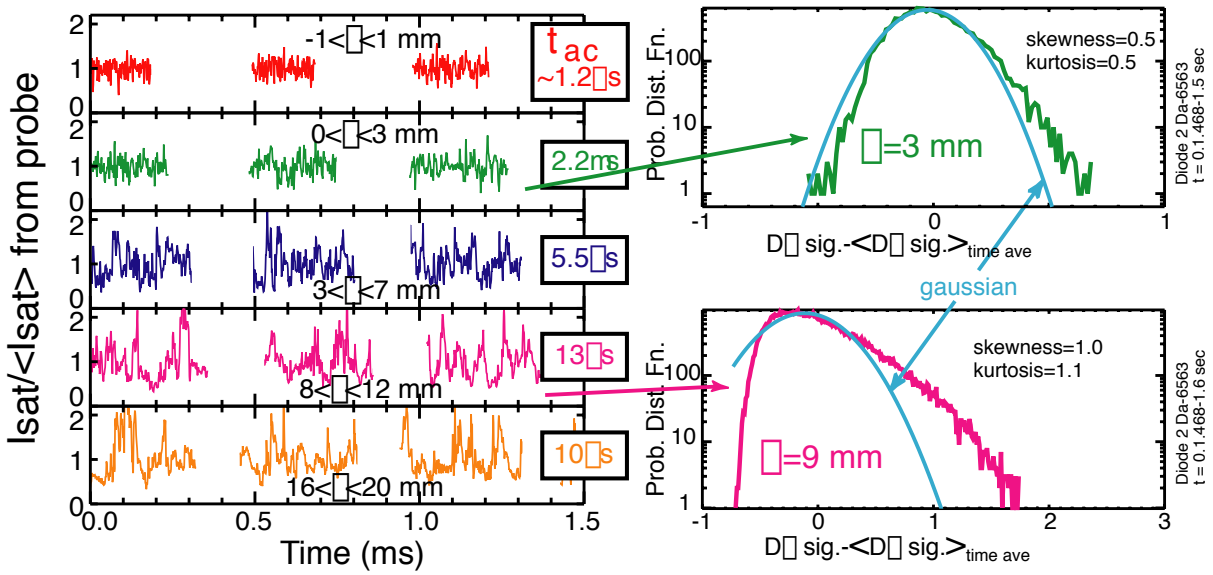
Isat/<Isat> from probe
-1<□<1 mm
0<□<3 mm
3<□<7 mm
8<□<12 mm
16<□<20 mm
t ac
~1.2□s
2.2ms
5.5□s
13□s
10□s
Time (ms)
Prob. Dist. Fn.
skewness=0.5
kurtosis=0.5
□=3 mm
D□ sig.-<D□ sig.>time ave
gaussian
skewness=1.0
kurtosis=1.1
□=9 mm
Diode 2 Da-6563
t = 0.1.468-1.5 sec
Diode 2 Da-6563
t = 0.1.468-1.6 sec

Figure 5

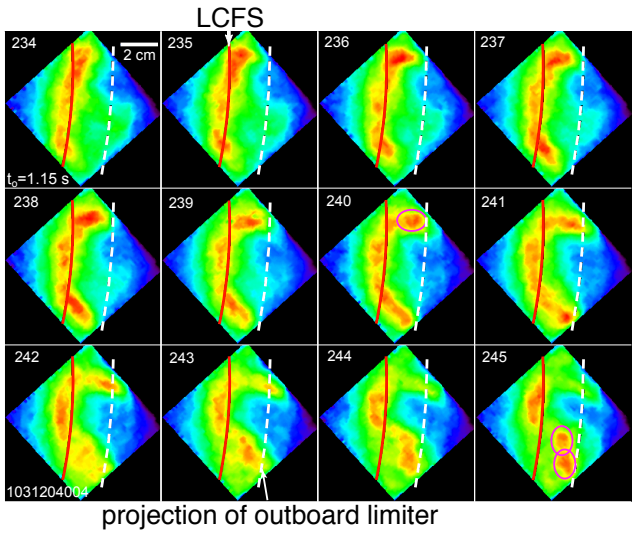
LCFS
234
2 cm
235
236
237
t_0=1.15 s
238
239
240
241
242
243
244
245
1031204004
projection of outboard limiter

Figure 6

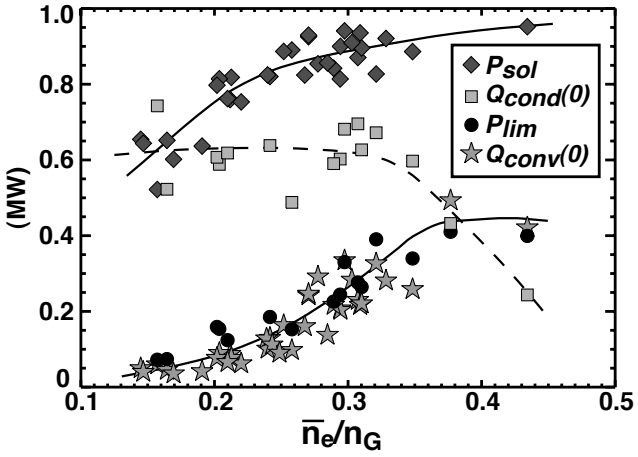
1.0
0.8
0.6
0.4
0.2
0
(MW)
0.1
0.2
0.3
0.4
0.5
$\bar{n}_e/n_G$
P_{sol}
$Q_{cond(0)}$
P_{lim}
$Q_{conv(0)}$

Figure 7

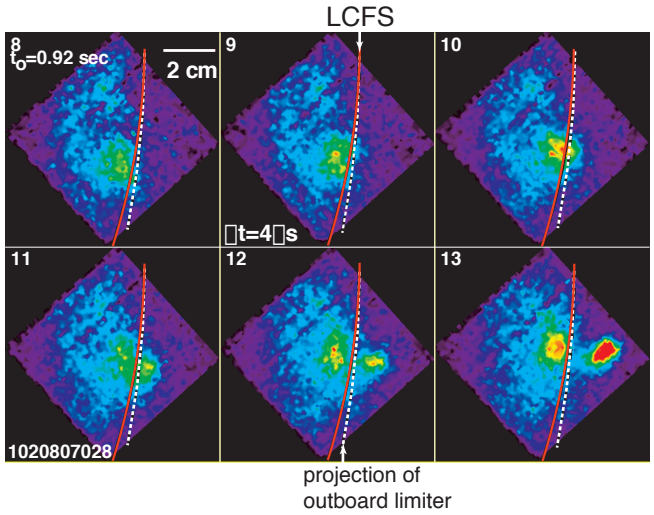
LCFS
8
t_o=0.92 sec
2 cm
9
10
□t=4□s
11
12
13
1020807028
projection of
outboard limiter

Figure 8

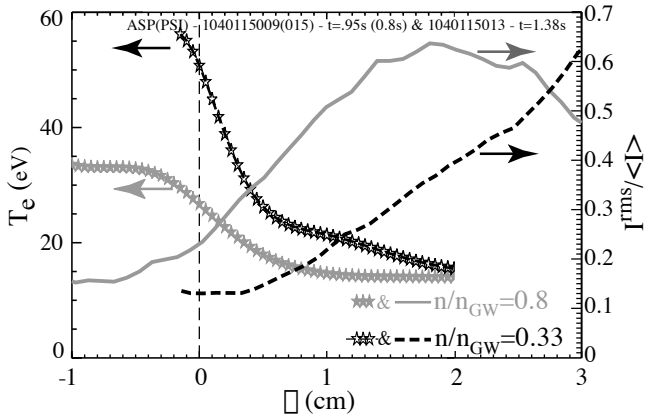
ASP(PSI) - 1040115009(015) - t=.95s (0.8s) & 1040115013 - t=1.38s
T_e (eV)
$I^{rms}/<I>$
□ (cm)
n/n$_{GW}$=0.8
n/n$_{GW}$=0.33

Figure 9

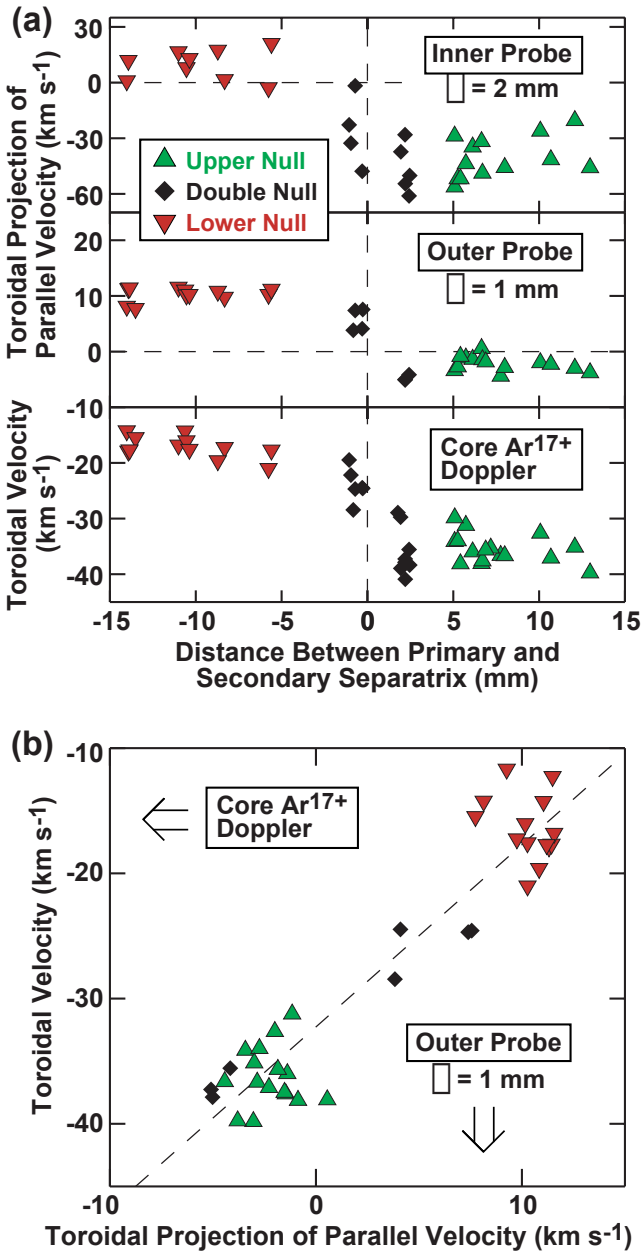
(a)
Inner Probe
= 2 mm
Upper Null
Double Null
Lower Null
Outer Probe
= 1 mm
Core Ar17+
Doppler
Toroidal Projection of
Parallel Velocity (km s-1)
Toroidal Velocity
(km s-1)
Distance Between Primary and
Secondary Separatrix (mm)
(b)
Core Ar17+
Doppler
Outer Probe
= 1 mm
Toroidal Velocity (km s-1)
Toroidal Projection of Parallel Velocity (km s-1)

Figure 10

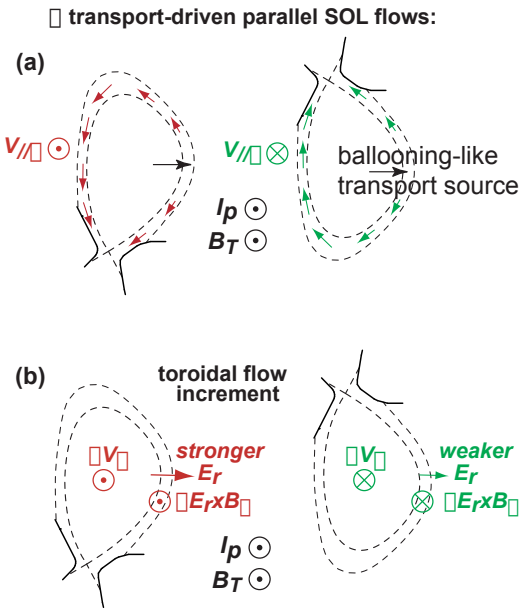
transport-driven parallel SOL flows:
(a)
V//
V//
ballooning-like
transport source
Ip
BT
(b)
toroidal flow
increment
V
stronger
Er
ErxB
V
weaker
Er
ErxB
Ip
BT

Figure 11

References

[1] B. LaBombard *et al.,* Nuclear Fusion **40** (2000) p 2041.
[2] M. Greenwald, Plasma Physics and Controlled Fusion **44** (2002) p R27-80.
[3] G. Counsell *et al.,* J Nucl Mater. **266-269** (1999) p 91.
[4] K. McCormick *et al.,* J Nucl Mater. **266** (1999) p 99-108.
[5] B. LaBombard *et al.,* J Nucl Mater. **220-222** (1995) p 976.
[6] B. LaBombard *et al.*, Phys. Plasmas **8** (2001) p 2107.
[7] J. Goetz *et al.*, Phys. Plasmas **3** (1996) p 1908.
[8] C.S. Pitcher *et al.,* Phys. Plasmas **7** (2000) p 1894.
[9] B. Lipschultz *et al.,* "Alcator C-Mod Neutrals", this issue of Fusion Sci. and Technol.
[10] B. LaBombard *et al.,* Phys. Plasmas **2** (1995) p 2242.
[11] B. LaBombard *et al.,* J Nucl Mater. **241-243** (1997) p 149.
[12] M. Umansky and B. LaBombard, J Nucl Mater. **266-269** (1999) p 721.
[13] B. LaBombard, Phys. Plasmas **9** (2002) p. 1300.
[14] B. Lipschultz *et al.,* Plasma Phys. Control. Fusion **47** (2005) p 1559.
[15] B. Lipschultz *et al.,* Proceedings of the 30th EPS Conference on Contr. Fusion and Plasma Physics, St. Petersburg **27A** (2003) P-3.197.
[16] M. Umansky *et al.,* Phys. Plasmas **5** (1998) p 3373.
[17] M. Umansky *et al.,* Phys. Plasmas **6** (1999) p 2791.
[18] B. Lipschultz *et al.,* Plasma Phys. Control. Fusion **44** (2002) p 733.
[19] D. Whyte *et al.,* Plasma Physics and Controlled Fusion 47 (2005) 1579.
[20] A. Loarte, Plasma Physics and Controlled Fusion 43 (2001) 183.
[21] J. Neuhauser *et al.,* Plasma Physics and Controlled Fusion, 16th European Physical Society Plasma Physics Division Conference on Controlled Fusion and Plasma Physics, 13-17 March 1989 31 (1989) 1551.
[22] K. McCormick *et al.,* in Controlled Fusion and Plasma Physics (Proc. 20th Eur. Conf., Lissabon, 1993), Vol. 2, European Physical Society, Geneva (1993) 587.
[23] H.S. Bosch *et al.,* J. Nucl. Mater. 220-220 (1995) 558.
[24] K. McCormick *et al.,* J. Nucl. Mater. 145-147 (1987) 215.
[25] G.K. McCormick and Z.A. Pietrzyk, J. Nucl. Mater. 162-164 (1989) 264.
[26] W.L. Rowan *et al.,* J. Nucl. Mater. 220-222 (1995) 668.
[27] M.E. Fenstermacher *et al.,* J. Nucl. Mater. 220-222 (1995) 330.
[28] J.G. Watkins *et al.,* J. Nucl. Mater. 220-222 (1995) 347.
[29] R.A. Moyer, J.W. Cuthbertson, T.E. Evans, G.D. Porter, J.G. and Watkins, J. Nucl. Mater. 241-243 (1997) 633.
[30] J.A. Boedo *et al.,* Phys. Plasmas 8 (2001) 4826.
[31] N. Asakura *et al.,* J. Nucl. Mater. 241-243 (1997) 559.
[32] S.K. Erents *et al.,* J. Nucl. Mater. 241-243 (1997) 433.
[33] J. Boedo *et al.,* Rev. Sci. Instrum. 69 (1998) 2663.
[34] R.A. Pitts *et al.,* J. Nucl. Mater. 290-293 (2001) 940.

[35] B. LaBombard LaBombard and B. Lipschultz "Cross-field transport in the SOL: its relationship to main chamber and divertor neutral control in Alcator C-Mod", *18th IAEA Fusion Energy Conf. (Sorrento, Italy, 2000)* IAEACN-77, EX5/6
[36] B.A. Carreras, *et al.,* Phys. Plasmas **8** (2001) p 3702.
[37] J.L. Terry *et al.,* J Nucl Mater. **290-293** (2001) p 757.
[38] S.J. Zweben *et al.,* Phys. Plasmas **9** (2002) p 1981.
[39] J.L. Terry *et al.,* Phys. Plasmas **10** (2003) p 1739.
[40] D.P. Stotler *et al.,* J Nucl Mater. **313-316** (2003) p 1066.
[41] R.J. Maqueda, *et al.,* Review of Scientific Instruments **74** (2003) p 2020.
[42] J.L. Terry *et al.*, Rev. of Scientific Instrum. **75** (2004) p 4196.
[43] J.L. Terry *et al.,* J Nucl Mater. **337-339** (2005) p 322.
[44] O. Grulke et al., Phys. Plasmas **13** (2006) 012306.
[45] J.L. Terry *et al.,* Nuclear Fusion **45** (2005) p 1321.
[46] B.N. Rogers *et al.*, PRL **81** (1998) p 4396.
[47] A. Zeiler *et al.,* Phys. Plasmas **5** (1998) p 2654.
[48] X.Q. Xu *et al.*, Phys. Plasmas **7** (2000) p 1951.
[49] X.Q. XU *et al.*, New Journal of Physics **4** (2002) p 53.
[50] M. Greenwald *et al.,* Nuclear Fusion **28** (1988) p 2199.
[51] B. LaBombard *et al.,* Nuclear Fusion **44** (2004) p 1047.
[52] N. Smick, B. LaBombard, and C.S. Pitcher, J. Nucl. Mater. **337-339** (2005) p 281.
[53] N.P. Basse *et al.,* "Diagnostic Systems on Alcator C-Mod", this issue of Fusion Sci. and Technol.
[54] C J Boswell *et al.,* Plasma Phys. Control. Fusion **46 (**2004) p 1247.
[55] B.L. Welch *et al.,* Phys. Plasmas **8** (2001) p 1253.
[56] J. Ghosh *et al.,* Phys. Plasmas **11** (2004) p 1033.
[57] B. LaBombard *et al.,* J Nucl Mater. **313-316** (2003) p 995.
[58] J. Rice *et al.,* Nuclear Fusion **41** (2001) p 277.